

## Hard-photon production and its correlation with intermediate-mass fragments in a framework of a quantum molecular dynamics model

S. S. Wang (王闪闪) <sup>1,2,3</sup> Y. G. Ma (马余刚) <sup>2,1,\*</sup> X. G. Cao (曹喜光) <sup>4,1</sup> D. Q. Fang (方德清)<sup>2,1</sup> and C. W. Ma (马春旺)<sup>5</sup>

<sup>1</sup>*Shanghai Institute of Applied Physics, Chinese Academy of Sciences, Shanghai 201800, China*

<sup>2</sup>*Key Laboratory of Nuclear Physics and Ion-beam Application (MOE), Institute of Modern Physics, Fudan University, Shanghai 200433, China*

<sup>3</sup>*School of Nuclear Sciences and Technology, University of Chinese Academy of Sciences, Beijing 100049, China*

<sup>4</sup>*Shanghai Advanced Research Institute, Chinese Academy of Sciences, Shanghai 201210, China*

<sup>5</sup>*Institute of Particle and Nuclear Physics, Henan Normal University, Xinxiang 453007, China*



(Received 20 February 2020; revised 14 May 2020; accepted 29 July 2020; published 17 August 2020)

Hard photon provides a unique probe for nuclear reaction dynamics. In this work, we embedded incoherent neutron-proton bremsstrahlung photon production channel in a framework of isospin-dependent quantum molecular dynamics (IQMD) model and performed a systematic study of multiplicities of hard photons and intermediate-mass fragments (IMFs). It is found that the IQMD model with the in-medium nucleon-nucleon cross section can reproduce previous experimental data of hard-photon energy spectra better. By investigating the incident energy and centrality dependencies of multiplicities of hard photons and IMFs of  $^{40}\text{Ca} + ^{40}\text{Ca}$  collisions, it is found that the multiplicity correlation between thermal photons and IMFs can provide valuable information on nuclear liquid-gas phase transition. Additionally, temperatures from the thermal emitting sources are also investigated. The results indicate that hard photons provide some unique information of the thermodynamical state of multifragmenting nuclear system.

DOI: [10.1103/PhysRevC.102.024620](https://doi.org/10.1103/PhysRevC.102.024620)

### I. INTRODUCTION

Heavy-ion collision, evolving from an early nonequilibrium state to a later phase of the de-excitation process, offers a unique possibility to investigate the properties of nuclear matter, especially to study the phase diagram of nuclear matter at changing densities and temperatures where a transition from the ground-state Fermi liquid drop to the nucleon gas phase was predicted [1–11]. Compared with nucleons, mesons, and charged particles emitted in the reactions, hard photons ( $E_\gamma > 30$  MeV) have a considerable advantage of not being disturbed by the final-state interactions except for weakly interacting with the surrounding nuclear medium through the electromagnetic interaction. In this context, hard photons provide a clean probe of the reaction dynamics and can deliver an unperturbed picture of the emitting source [12–20]. That is a reason why hard-photon emission in intermediate-energy heavy-ion collisions has attracted great attention since they have been observed in experiments [21]. Moreover, extreme high-energy hard photon being as a unique probe for the properties of quark-gluon plasma has been extensively investigated in the ultrarelativistic heavy-ion collision community [22–26].

Many efforts have been made to understand the hard-photon production mechanism in heavy-ion collision both experimentally [27–32] and theoretically [33–42]. From these

studies, it was well established that the hard photons are primarily produced from the incoherent bremsstrahlung of energetic nucleons. Because destructive interference of the hard photons emitted from two protons makes the photon production cross section much smaller than that from neutron-proton collisions, the latter process ( $n + p \rightarrow n + p + \gamma$ ) is often treated as the main source of hard photons in theoretical works. In addition, it has been pointed out and demonstrated that hard photons originated from two distinct sources (i.e., direct photon and thermal photon sources) in space and time according to the experimental evidence as well as the Boltzmann-Uehling-Uhlenbeck (BUU) model calculations [43,44]. Direct photons stem from the first compression phase in the early stage of the reaction, corresponding to the first-chance neutron-proton collisions, which account for the dominant contribution. Thermal photons are emitted from a thermalized source during the later stage of the reaction, which are softer than direct photons in energy spectra.

Different from experimental method of distinguishing direct photons from thermal photons, they have been discriminated from the time evolution in Refs. [15,16] within the BUU model. Although some intriguing features on direct and thermal photons were explored, an almost constant time evolution of thermal photon production probability seems not reasonable because of fragment formation during the later stage of the reaction system. So in this article, we introduce the hard-photon production channel into an isospin-dependent quantum molecular dynamics (IQMD) model which has been

\*Corresponding author: mayugang@fudan.edu.cn

successfully applied to various aspects of heavy-ion physics in the intermediate-energy region. For the process of two-body collision in this model, the in-medium nucleon-nucleon cross section from Refs. [45,46] is employed instead of free nucleon-nucleon cross section.

The rest of this paper is arranged as follows: In Sec. II, we briefly describe the IQMD model, the in-medium nucleon-nucleon cross section, and the formula of hard-photon production probability. Results and discussion are described in Sec. III, where we compare our calculations with the experimental data and present the incident energy and centrality dependence of the multiplicities of direct photons, thermal photons, and intermediate-mass fragments (IMFs), respectively. In addition, we also demonstrate the characteristics of multiplicity correlation between hard photons and IMFs and briefly discuss the thermometer of hard photons in this section. Finally, Sec. IV gives a summary.

## II. MODEL AND FORMALISM

### A. Brief introduction of the IQMD model

The IQMD model is an isospin-dependent QMD model and was very successful in describing intermediate-energy heavy-ion collisions [11,47–57]. The total wave function for the  $N$ -body system in this model is treated as a direct product of Gaussian wave function of all nucleons with wave packet width  $L = 2.16 \text{ fm}^2$  [47],

$$\Phi(\mathbf{r}, t) = \prod_i^N \phi_i(\mathbf{r}, t), \quad (1)$$

where  $\phi_i(\mathbf{r}, t)$  represents the Gaussian wave packet function of the  $i$ th nucleon,

$$\phi_i(\mathbf{r}, t) = \frac{1}{(2\pi L)^{3/4}} \exp\left[-\frac{(\mathbf{r} - \mathbf{R}_i)^2}{4L} + \frac{i\mathbf{P}_i \cdot \mathbf{r}}{\hbar}\right]. \quad (2)$$

Here  $\mathbf{R}_i$  and  $\mathbf{P}_i$  are the centers of position and momentum of the  $i$ th wave packet, respectively.

In the model, the Pauli blocking is considered as follows. One assumes that each nucleon occupies a sphere with a volume of  $h^3/2$  in coordinate and momentum space. Whenever a collision happens, one only needs to calculate the phase-space volume,  $V$ , of the each scattered nucleon being occupied by the rest nucleons with the same isospin and then decide whether the collision is blocked or not by comparing  $2V/h^3$  with a random number. As a result, the probability of this collision being blocked is taken as

$$P_{\text{block}} = 1 - (1 - P_1)(1 - P_2), \quad (3)$$

where  $P_1$  and  $P_2$  are the blocking probabilities of the scattered nucleons. They are calculated from an overlap of hard spheres as

$$P_i = \sum_{k \neq i} \frac{O_{ik}^x}{\frac{4}{3}\pi R_x^3} \frac{O_{ik}^p}{\frac{4}{3}\pi R_p^3}, \quad i = 1, 2, \quad (4)$$

where  $O_{ik}^x$  and  $O_{ik}^p$  are the volume of the overlap region of hard spheres with the radius  $R_x$  and  $R_p$  of the scattered nucleons  $i$  in the coordinate and momentum space and the latter relates to

the local density, i.e.,  $R_p = (\frac{3\pi^2}{2}\rho)^{1/3}$  and  $(\frac{4}{3}\pi R_x^3)(\frac{4}{3}\pi R_p^3) = h^3/2$ . It is known that QMD models generally have an unavoidable problem to underestimate the blocking probability because of fluctuations [58]. In order to check the blocking effects in this work, we performed some box calculations with the same setting as in Ref. [58]. The average numbers of attempted collisions and successful collisions over the time interval 60–140 fm/c without nuclear mean field and no Coulomb interactions for temperature  $T = 5 \text{ MeV}$  initialization are obtained as 118.7 c/fm and 9.9 c/fm, respectively, which are comparable with that from the BUU approaches. So the Pauli blocking procedure in this IQMD model seems reasonable.

### B. In-medium nucleon-nucleon cross section

It was known that in-medium effects cannot be ignored in intermediate-energy heavy-ion collisions [59] and several forms of the in-medium nucleon-nucleon cross section (in-medium NNCS) were available [45,60,61]. Here we employ the screened cross section as the in-medium NNCS in the process of nucleon-nucleon scattering in the IQMD model. It is derived from the geometric reasoning that the geometric cross-section radius should not exceed the interparticle distance and is implemented in the form [45,46]

$$\sigma_{NN}^{\text{in-medium}} = \sigma_0 \tanh(\sigma_{NN}^{\text{free}}/\sigma_0), \quad (5)$$

$$\sigma_0 = y\rho^{-2/3}, \quad y = 0.85. \quad (6)$$

Here  $\rho$  denotes the single-particle density and  $\sigma_{NN}^{\text{free}}$  represents the free nucleon-nucleon cross section (free NNCS) parametrization from experimental measurements [62].

### C. Hard-photon production probability

As mentioned, the IQMD model was very successful to investigate nuclear reaction dynamics and nuclear matter properties in intermediate-energy heavy-ion collision. This is why we want to introduce hard-photon production channel into the IQMD model. According to the main mechanism of hard-photon production in intermediate-energy heavy-ion collisions, which is incoherent bremsstrahlung from individual  $n$ - $p$  collisions [38–41], the elementary double differential hard-photon production cross section in the nucleon-nucleon center-of-mass frame is described by employing the hard-sphere collision limit from Ref. [63] and modified as in Ref. [41] for energy conservation,

$$\frac{d^2\sigma^{\text{elem}}}{dE_\gamma d\Omega_\gamma} = \alpha_c \frac{R^2}{12\pi} \frac{1}{E_\gamma} (2\beta_f^2 + 3\sin^2\theta_\gamma \beta_i^2), \quad (7)$$

where  $\alpha_c$  is the fine structure constant,  $R$  is the radius of hard sphere, and  $E_\gamma$  is the energy of emitting photon.  $\beta_i$  and  $\beta_f$  are the initial and final velocity of the proton, and  $\theta_\gamma$  is the angle between the momenta of the incident particle and the emitted photon. The hard-photon production probability in a heavy-ion collision is obtained by summing the contributions from all  $n$ - $p$  collisions at each time step and integrating over the direction  $\Omega_e$  of the relative momenta between the final nucleons. The hard-photon production probability in the

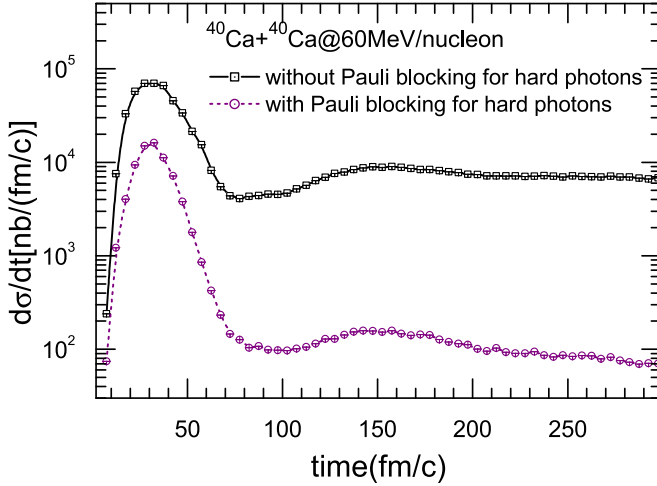


FIG. 1. Time evolution of differential cross section from inclusive events of  $^{40}\text{Ca} + ^{40}\text{Ca}$  at 60 MeV/nucleon, including with (purple circles) and without Pauli blocking (black squares) for hard photons.

nucleus-nucleus center-of-mass frame can be derived from Eq. (7),

$$\frac{d^2N(b)}{dE_\gamma d\Omega_\gamma} = \sum_{pncoll} \int \frac{d\Omega_e E_\gamma}{4\pi E'_\gamma} \frac{1}{\sigma_{NN}} \frac{d^2\sigma^{elem}}{dE'_\gamma d\Omega'_\gamma}(\mathbf{k}_1 - \mathbf{k}_2)[1 - P_{block}]. \quad (8)$$

Here primed quantities are in the nucleon-nucleon center-of-mass frame and unprimed quantities are in the nucleus-nucleus center-of-mass frame.  $\sigma_{NN}$  denotes the total nucleon-nucleon cross section and equals  $\pi R^2$  where  $R$  is the radius of the hard sphere in Eq. (7). The in-medium effect is also taken into account in the process of  $n + p \rightarrow n + p + \gamma$  by checking the collision distance  $\sqrt{\sigma_{NN}^{in-medium}/\pi}$ . The last term represents the effects of Pauli blocking in the final state phase space, which can be obtained by Eqs. (3) and (4). More information can be found in Refs. [40–42].

It should be mentioned that the hard-photon emission channel is regarded as a perturbation because the production of hard photons is relatively rare, which means that the production of hard photons does not take away energy and momentum from the reaction system. So in order to check the effect of Pauli blocking on photon production, one just needs to switch on and switch off the process of the Pauli blocking for hard photons that does not affect the reaction system. Figure 1 shows the time evolution of differential cross section ( $d\sigma/dt$ ) of hard photons, including with and without the Pauli blocking for inclusive events of  $^{40}\text{Ca} + ^{40}\text{Ca}$  at 60 MeV/nucleon. It is found that the Pauli blocking also plays a significant role for hard-photon production, especially for that emission at the later stage of reaction.

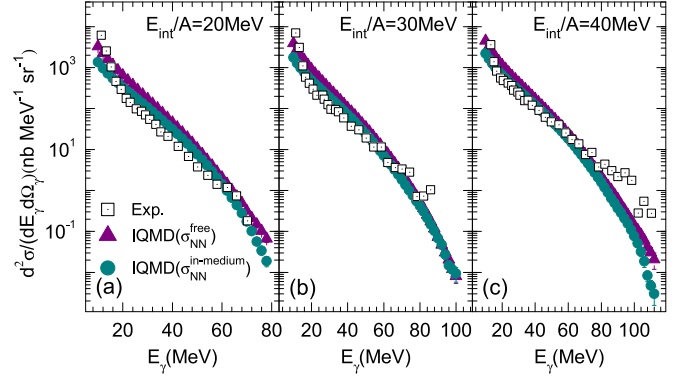


FIG. 2. Photon energy spectra at  $\theta_{lab}$  around  $90^\circ$  for the reaction  $^{14}\text{N} + ^{12}\text{C}$  at incident energies of 20 (a), 30 (b), and 40 (c) MeV/nucleon. Open square represents the experimental data from Ref. [29]. Solid triangle and circle correspond to our simulation results from the IQMD model with the free and in-medium NNCS, respectively.

### III. RESULTS AND DISCUSSION

#### A. Comparison between experimental data and calculated photon energy spectra

In this section, both experimental and calculated photon energy spectra for the reaction of  $^{14}\text{N} + ^{12}\text{C}$  at incident energies of 20 MeV/nucleon (a), 30 MeV/nucleon (b), and 40 MeV/nucleon (c) are shown in Fig. 2. Open square represents experimental data from Ref. [29], and solid triangle and solid circle depict the calculated results in the framework of IQMD model with the free NNCS and in-medium NNCS, respectively. From this comparison, we see that the calculated results employing the in-medium NNCS in the IQMD model is in good agreement with the experimental data, which illustrates that the in-medium effect plays a significant role in intermediate-energy heavy-ion collision. Hence the following calculations are obtained based on the IQMD model with the in-medium NNCS.

#### B. Definitions of direct photon and thermal photon

It is well established that hard photons which include direct photons and thermal photons are emitted from two distinct sources in intermediate-energy heavy-ion collision, which has been mentioned in Sec. I. How to separate direct photon and thermal photon, and how to define the separation time ( $t_s$ ) between them, is important in this model calculation. Here it is realized that direct photon is produced during the first compression-expansion stage in the time evolution process of the system, and thermal photon is emitted from a thermalized source during the second compression-expansion stage. Based on this definition,  $t_s$  can be obtained from the time evolution of average density.

Usually the average density increases during the first compression stage of reaction system and then decreases with the system expansion up to the minimum around 100 fm/c. After that, there is a second compression-expansion phase. The moment corresponding to the minimum average density can be labeled as  $t_s$  to distinguish direct photons from thermal

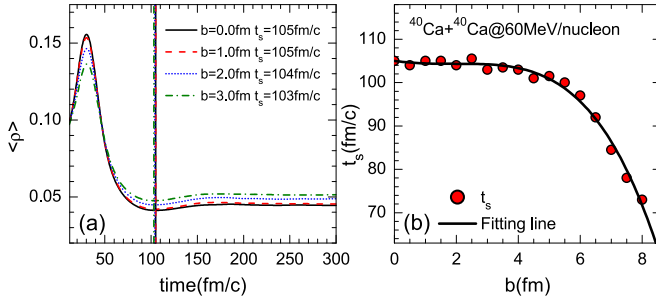


FIG. 3. (a) Time evolution of the average density in the reaction of  $^{40}\text{Ca} + ^{40}\text{Ca}$  at an incident energy of 60 MeV/nucleon. (b) Separation time between direct photons and thermal photons as a function of impact parameter. Line is the fitting curve with a polynomial function.

photons. For example, it is found from Fig. 3(a) that  $t_s = 105, 105, 104,$  and  $103$  fm/c correspond to impact parameters 1.0, 2.0, 3.0, and 4.0 fm, respectively, for the reaction of  $^{40}\text{Ca} + ^{40}\text{Ca}$  at 60 MeV/nucleon. Except for impact parameter, incident energy ( $E_{\text{int}}/A$ ) is another factor to determine  $t_s$  for the reaction system. To obtain  $t_s$  for every event, we first obtain the impact parameter dependence of separation time at a given incident energy and fit it as a function of impact parameter. As an example, Fig. 3(b) gives  $t_s$  as a function of  $b$  for  $^{40}\text{Ca} + ^{40}\text{Ca}$  at 60 MeV/nucleon, in which the line is the fitting curve with a polynomial function up to fourth order. Once such a fitting function is determined, we can obtain  $t_s$  at each  $b$  for a given  $E_{\text{int}}/A$  and then use this value to distinguish thermal photons from direct photons.

### C. Multiplicities of direct photons and thermal photons

In this section, we investigate the multiplicity dependence of direct and thermal photons on incident energy and centrality in the framework of the IQMD model taking into account the in-medium effects, respectively. As in a traditional way, the centrality to which a certain range of impact parameter  $b$  corresponds can be defined by  $\frac{\pi b^2}{\pi b_{\text{max}}^2}$ . With this definition, smaller centrality corresponds to more central collisions, and larger centrality means peripheral collisions.

Figures 4(a) and 4(b) show the multiplicities of direct ( $M_\gamma^d$ ) and thermal ( $M_\gamma^{\text{th}}$ ) photons as a function of  $E_{\text{int}}/A$  in  $^{40}\text{Ca} + ^{40}\text{Ca}$  in different centralities, respectively. We can see that in most cases the multiplicities of direct and thermal photons monotonously increase with  $E_{\text{int}}/A$  at different centralities. However, for thermal photons emitted from the cases at centrality 0–20%, their multiplicities have a decreasing tendency with increasing  $E_{\text{int}}/A$  and then reach a saturation around  $M_\gamma^{\text{th}} = 4.43 \times 10^{-6}$  when  $E_{\text{int}}/A$  is larger than 80 MeV. The interpretation is that there is a fierce competition between thermal photon emission and multifragment emission in central collisions as a function of  $E_{\text{int}}/A$ . The suppression of thermal photon emission is because that multifragment production reduces the chance of  $n$ - $p$  collision, while higher  $E_{\text{int}}/A$  collision favors to produce more light particles rather than IMFs and then contributes to a little more thermal photon production. Later we can actually see the rise and

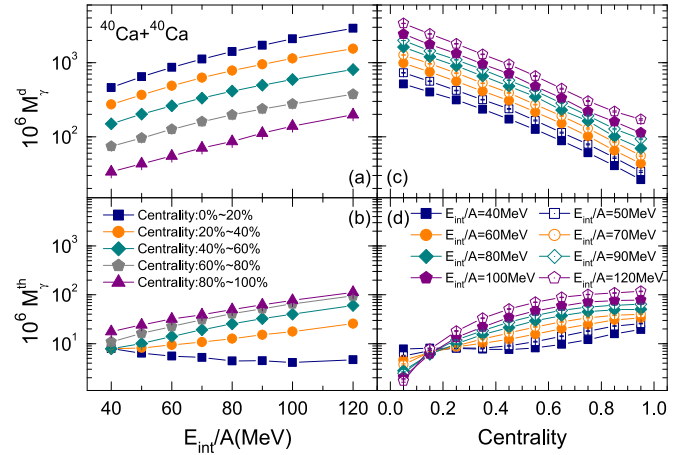


FIG. 4. Multiplicities of direct and thermal photons as functions of incident energy and centrality in the reaction of  $^{40}\text{Ca} + ^{40}\text{Ca}$ , respectively. Panels (a) and (b) represent direct photon multiplicity ( $M_\gamma^d$ ) and thermal photon multiplicity ( $M_\gamma^{\text{th}}$ ) versus  $E_{\text{int}}/A$ , respectively, while (c) and (d) depict  $M_\gamma^d$  and  $M_\gamma^{\text{th}}$  versus centrality, respectively.

fall behavior for the IMFs' multiplicity in central collisions (Fig. 5). Moreover, one can see another phenomenon for different centralities at the same  $E_{\text{int}}/A$ , where the more direct photons are produced, the fewer thermal photons are emitted.

Figures 4(c) and 4(d) display the multiplicities of direct and thermal photons as a function of centrality at different incident energies, respectively. We can see that there is a monotonously decreasing tendency with the increasing of centrality for direct photons, indicating that there are much more first  $n$ - $p$  collision probability in more central collisions because of the much bigger size of interaction zone. Conversely, the multiplicity of thermal photons emitted from central collision is much less than that from peripheral collisions, especially for the reaction at higher  $E_{\text{int}}/A$ . This phenomenon also results from more multifragment production in more central collisions at higher  $E_{\text{int}}/A$  collisions which makes the chance of  $n$ - $p$  collision decreases at the later stage of reaction.

Based on the above study, direct photons always show a monotonous variation as a function of  $E_{\text{int}}/A$  and centrality,

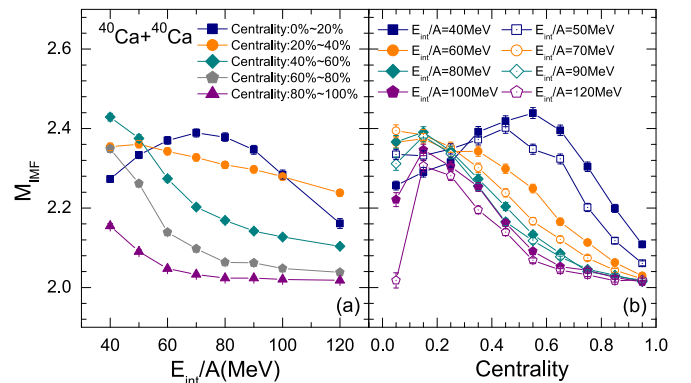


FIG. 5. Multiplicity of IMFs as a function of incident energy (a) and centrality (b) in the reaction of  $^{40}\text{Ca} + ^{40}\text{Ca}$ , respectively.

which makes direct photons hard to be a good probe to study the liquid-gas phase transition in intermediate-energy heavy-ion collisions.

#### D. Multiplicities of IMFs

The intermediate-mass fragments multiplicities have been extensively investigated in recent years. It is suggested that a large number of IMFs are emitted when nuclear liquid-gas phase transition happens [3,5,7–10], and therefore the multiplicity of IMFs is often taken as an important observable for exploring nuclear liquid-gas phase transition in heavy-ion collisions.

In this work, we define IMF as the fragment with  $Z \geq 3$ . In Fig. 5(a), incident energy dependence of IMFs' multiplicity is shown for  $^{40}\text{Ca} + ^{40}\text{Ca}$  collisions. It is found that there is a rise and fall of IMFs' multiplicity [3,64,65] at centrality of 0–20%, and a maximum value takes place at  $E_{\text{int}}/A = 70$  MeV. It indicates that nuclear liquid-gas phase transition could occur for  $^{40}\text{Ca} + ^{40}\text{Ca}$  system around 70 MeV/nucleon in central collisions. On the other hand, IMFs' multiplicities monotonously decrease with the increasing of  $E_{\text{int}}/A$  for more peripheral collisions. In addition, IMFs' multiplicities as a function of centrality are plotted with fixed  $E_{\text{int}}/A$  from 40 to 120 MeV in Fig. 5(b), which essentially displays similar rise and fall tendency.

#### E. Multiplicities correlation between hard photons and IMFs

The correlation between hard photons and IMFs was discussed for reaching a comprehensive understanding of their emission mechanism [66]. The correlation factor is defined as the following:

$$1 + R_{\gamma\text{-IMF}} = \frac{\langle M_{\gamma} M_{\text{IMF}} \rangle}{\langle M_{\gamma} \rangle \langle M_{\text{IMF}} \rangle}, \quad (9)$$

where  $\langle M_{\gamma} \rangle$  and  $\langle M_{\text{IMF}} \rangle$  denote average multiplicities of hard photons and IMFs, respectively.  $M_{\gamma}$  and  $M_{\text{IMF}}$  are produced from the same event in terms of  $\langle M_{\gamma} M_{\text{IMF}} \rangle$ . If the correlation factor is less than 1.0, then it indicates an anticorrelation between the hard photons and IMFs, which means a competition between them. If the hard-photon emission and IMFs production are positively correlated, then the factor should be larger than 1.0.

First let us check the time evolution of multiplicity correlation between the hard photons and IMFs. An example is given for inclusive events of  $^{40}\text{Ca} + ^{40}\text{Ca}$  reaction at 60 MeV/nucleon, which is shown in Fig. 6. Figures 6(a) and 6(b) display the time evolution of hard-photon production probability and IMFs, respectively. Their correlation factor is shown in Fig. 6(c). As mentioned, hard photons could be produced during the whole reaction process once there are enough neutron-proton collisions. For IMFs, they are formed at around 60 fm/c and increase quickly afterward and then tend to saturate. For their correlation factor, it shows a turning point from positive to negative correlation where  $R_{\gamma\text{-IMF}}$  is equal to 1.0 at time of the first minimum of the photon production probability as well as the maximum value of IMFs. A positive correlation between the direct hard photon and IMFs

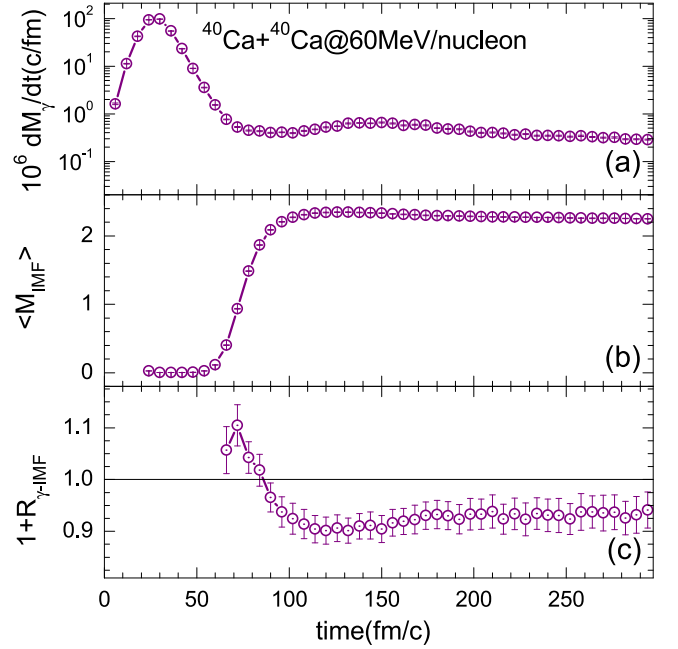


FIG. 6. Time evolutions of photon production probability (a), IMFs (b), and the multiplicity correlation between them (c) for inclusive events of 60 MeV/nucleon  $^{40}\text{Ca} + ^{40}\text{Ca}$ .

at the earlier stage of reaction illustrates that first-channel hard photon could be coherently produced with the IMFs when the reaction system is still hot enough. With the reaction system entering into expansion stage, the thermal hard photon could be produced due to subsequent neutron-proton collisions in hot fragments. However, the fragments have to be hot enough so that the neutron-proton collisions are sufficiently energetic to produce hard photons. In this context, an anticorrelation between the thermal hard photon and IMFs emerges at the later stage of reaction. It also indicates that there exists a competition between them.

From experimental aspects, time evolution is difficultly accessible since usually we have only freeze-out products, so the correlation factors can only be performed by the hard photons and final-state IMFs. Supposing that direct photons which are emitted during the earlier stage of heavy-ion collision is independent of IMFs which are mostly produced at the later stage, the correlation factor should be then close to 1.0, i.e., no correlation. In order to check it, Figs. 7(a) and 7(c) show the multiplicity correlation between direct photons and IMFs as a function of  $E_{\text{int}}/A$  and centrality for  $^{40}\text{Ca} + ^{40}\text{Ca}$  collisions, respectively. It is clearly seen that  $|R_{\gamma\text{-IMF}}|$  is almost zero, which indicates that the absence of any turning point or structure with the energy or centrality evolution viewing from the multiplicity correlation between the direct photons and IMFs, and therefore it cannot be taken as a probe to investigate the nuclear liquid-gas phase transition.

On the other side, the multiplicity correlation between the thermal photons and IMFs could be promising. Figures 7(b) and 7(d) show this correlation as a function of  $E_{\text{int}}/A$  and centrality for  $^{40}\text{Ca} + ^{40}\text{Ca}$  collisions, respectively. Overall, they demonstrate values of less than 1 for  $1 + R_{\gamma\text{-IMF}}$ ,

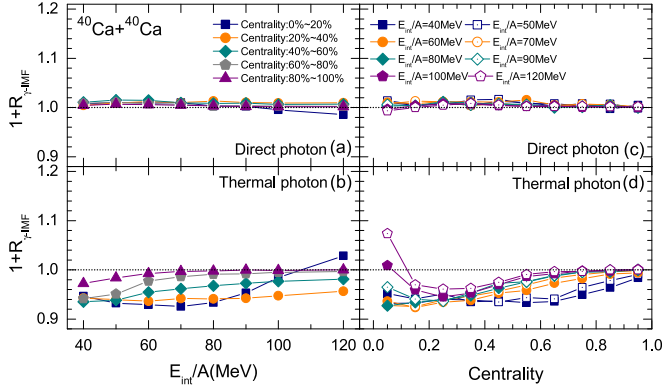


FIG. 7. Multiplicity correlation between the direct photons [(a) and (c)] or thermal photons [(b) and (d)] and IMFs as a function of incident energy and centrality, respectively, in the reaction of  $^{40}\text{Ca} + ^{40}\text{Ca}$  collisions.

indicating a competition between the IMFs' emission and thermal photons' emission. The values of  $|R_{\gamma-IMF}|$  for the correlation of thermal photons with IMFs, varying from 0% to 8%, are much larger than that for the correlation of the direct photons with IMFs, which means that there is indeed a stronger anticorrelation between the thermal photon emission and IMF production in intermediate-energy heavy-ion collision. This phenomenon can be understood whereby both thermal photons and IMFs are produced during similar later stages of the collision, and the IMF production inhibits thermal photon yield. Moreover, it is also seen from Fig. 7(b) that there is a fall and rise tendency for the correlation factor ( $1 + R_{\gamma-IMF}$ ) between thermal photons and IMFs with the increasing of  $E_{int}/A$  at centrality 0–20%. And a broad dip of the correlation factor appears at  $E_{int}/A = 70$  MeV, which is consistent with a phenomenon of nuclear liquid-gas phase transition from a peak of IMF multiplicity at  $E_{int}/A = 70$  MeV in the centrality of 0–20%. For centrality dependence of  $1 + R_{\gamma-IMF}$ , their trends also follow the behavior of IMFs' multiplicity as shown in Fig. 5(b) but just with the reverse trend.

### F. Thermometer of hard photons

In addition to the correlation signal from the hard photons and IMFs, the hard photons can also be treated as the thermometers for both pre-equilibrium system and excited nuclear residues. For example, Ref. [67] discussed slopes of the direct and thermal photons of four different heavy-ion reactions at intermediate bombarding energies with the two-arm photon spectrometer (TAPS), and Ref. [68] extracted the temperature  $T$  from the emitting source by an exponential fit to the thermal photon spectra and obtained a caloric curve. In the present calculations, we can also extract the slope parameters for the direct and thermal components from inclusive events in the reaction of  $^{40}\text{Ca} + ^{40}\text{Ca}$ . First, as an example, Fig. 8(a) shows the energy spectra of the direct photons and thermal photons at 60 MeV/nucleon for inclusive events of 60 MeV/nucleon  $^{40}\text{Ca} + ^{40}\text{Ca}$  collisions. Lines are the fitting curves with an

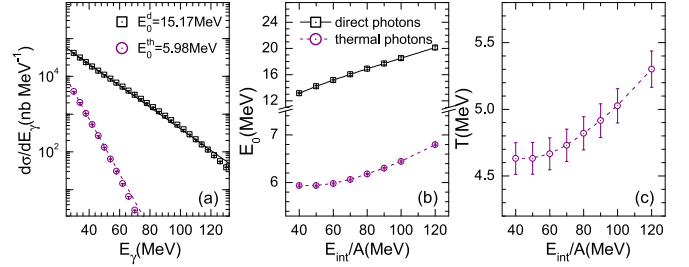


FIG. 8. (a) Hard-photon energy spectra for inclusive events of the reaction of  $^{40}\text{Ca} + ^{40}\text{Ca}$  at 60 MeV/nucleon. Squares and circles represent the direct photons and thermal photons, respectively. Lines are the exponential fitting with Eq. (10). (b) The inverse slope parameters of the direct photons (squares) and thermal photons (circles) as a function of incident energy. (c) Temperatures extracted from a thermal photon thermometer [Eq. (11)] as a function of incident energy.

exponential function as

$$\frac{d\sigma}{dE_\gamma} = K e^{-\frac{E_\gamma}{E_0}}, \quad (10)$$

where  $K$  is a fitting constant and  $E_0$  represents inverse slope parameter. The slope parameter is 15.17 and 5.98 MeV, respectively, corresponding to those of the direct photons ( $E_0^d$ ) and thermal photons  $E_0^{\text{th}}$ . Then the slope parameters  $E_0$  as a function of  $E_{int}/A$  are plotted in Fig. 8(b). It can be found that  $E_0$  increases from 13.2 to 20.1 MeV with  $E_{int}/A$  for the direct photons, and for the thermal photons the slopes are much smaller than those of direct photons which also increase with  $E_{int}/A$  in a range of 5.9–6.8 MeV. Finally, according to an empirical relation between the temperature  $T$  of the emitting source and  $E_0^{\text{th}}$  of thermal photons [68],

$$T = (0.78 \pm 0.02)E_0^{\text{th}}, \quad (11)$$

we obtained the thermal source temperatures increasing from 4.6 to 5.3 MeV with  $E_{int}/A$ , which are plotted in Fig. 8(c). These above results are similar to those from Refs. [67–69]. Therefore the hard photon slopes become good probes for the “thermal” indication of pre-equilibrium emission as well as the temperature of the excited nuclear residues remaining after the first pre-equilibrium phase of the reaction, providing some unique information of the thermodynamical state of multifragmenting nuclear system [68].

## IV. SUMMARY

In summary, the IQMD model was calculated by embedding incoherent neutron-proton bremsstrahlung photon production channel in order to investigate high-energy photon production and its correlation with fragments in this work. A systematic study of the multiplicities of hard photons and intermediate-mass fragments in the reaction of  $^{40}\text{Ca} + ^{40}\text{Ca}$  was performed with the IQMD concerning the in-medium nucleon-nucleon cross-section effect in nuclear matter. By comparing the calculated results with the experimental data, we found that the IQMD model with the in-medium nucleon-nucleon cross section can better reproduce the experimental

hard-photon energy spectra. Based on the production mechanism of direct photons and thermal photons, which the former is emitted during the first compression-expansion stage in the time evolution process of the system and the latter is produced during the second compression-expansion stage, a separation time ( $t_s$ ) between them is obtained from the time evolution of average density. In order to get the  $t_s$  for every event, a fitting function with a polynomial function up to fourth order is used to fit  $t_s$  as a function of impact parameter at a given incident energy ( $E_{\text{int}}/A$ ). Then we investigated the incident energy and centrality dependencies of the multiplicities of the direct photons, thermal photons, and IMFs, respectively. It is found that the multiplicity of the direct photons varies monotonically with beam energy as well as centrality, which makes it difficult to search for the turning point induced by nuclear liquid-gas transition by using the direct photon as a probe alone. But for IMFs, their average multiplicity appears a rise and fall tendency with the increasing of  $E_{\text{int}}/A$  at 0–20% central collisions, implying that there occurs the nuclear liquid-gas phase transition. Finally, the study on the multiplicity correlation between the hard photons and IMFs was proceeded, and a very weak correlation between direct photons and IMFs was observed. However, for the thermal photons, the multiplicity correlation is much stronger with the IMFs, and the correlation factor just takes the reverse tendency with the increasing of  $E_{\text{int}}/A$  as the multiplicity of IMFs at centrality 0–20%, which supports our argument that there exists the nuclear liquid-gas transition at  $E_{\text{int}}/A =$

70 MeV  $^{40}\text{Ca} + ^{40}\text{Ca}$  collisions at this centrality. Therefore the multiplicity correlation between the thermal photon and IMFs can be taken as a probe to study the nuclear liquid-gas phase transition in intermediate energy heavy-ion collision. Additionally, the thermometer of hard photons was also investigated. It is found that the temperature from the thermal emitting sources varies in the range of 4.6–5.3 MeV, which is similar to experimental results of other systems. It indicates that hard photons can be regarded as a unique tool to study the thermodynamical state of a multifragmenting nuclear system.

#### ACKNOWLEDGMENTS

This work was supported in part by the National Natural Science Foundation of China under Contracts No. 11890714, No. 11421505, No. 11925502, No. 11305239, No. 11220101005, and No. 1961141003; the Strategic Priority Research Program of the Chinese Academy of Sciences under Grants No. XDB34030200 and No. XDB16; the Major State Basic Research Development Program in China under Contract No. 2014CB845401; the Youth Innovation Promotion Association CAS under Grant No. 2017309; the Program for Science and Technology Innovation Talents in Universities of Henan Province under Grant No. 13HASTIT046; and Natural and Science Foundation in Henan Province under Grant No. 162300410179.

- 
- [1] B. Borderie and J. D. Frankland, *Prog. Part. Nucl. Phys.* **105**, 82 (2019).
- [2] C. W. Ma and Y. G. Ma, *Prog. Part. Nucl. Phys.* **99**, 120 (2018).
- [3] Y. G. Ma and W. Q. Shen, *Phys. Rev. C* **51**, 710 (1995).
- [4] J. Pochodzalla *et al.*, *Phys. Rev. Lett.* **75**, 1040 (1995).
- [5] Y. G. Ma, *Phys. Rev. Lett.* **83**, 3617 (1999).
- [6] J. B. Natowitz, K. Hagel, Y. G. Ma, M. Murray, L. Qin, R. Wada, and J. Wang, *Phys. Rev. Lett.* **89**, 212701 (2002).
- [7] Y. G. Ma, J. B. Natowitz, R. Wada, K. Hagel, J. Wang, T. Keutgen, Z. Majka, M. Murray, L. Qin, P. Smith, R. Alfaro, J. Cibor, M. Cinausero, Y. El Masri, D. Fabris, E. Fioretto, A. Keksis, M. Lunardon, A. Makeev, N. Marie, E. Martin, A. Martinez-Davalos, A. Menchaca-Rocha, G. Nebbia, G. Prete, V. Rizzi, A. Ruangma, D. V. Shetty, G. Souliotis, P. Staszal, M. Veselsky, G. Viesti, E. M. Winchester, and S. J. Yennello, *Phys. Rev. C* **71**, 054606 (2005).
- [8] Y. G. Ma, R. Wada, K. Hagel, J. Wang, T. Keutgen, Z. Majka, M. Murray, L. Qin, P. Smith, J. B. Natowitz, R. Alfaro, J. Cibor, M. Cinausero, Y. El Masri, D. Fabris, E. Fioretto, A. Keksis, M. Lunardon, A. Makeev, N. Marie, E. Martin, A. Martinez-Davalos, A. Menchaca-Rocha, G. Nebbia, G. Prete, V. Rizzi, A. Ruangma, D. V. Shetty, G. Souliotis, P. Staszal, M. Veselsky, G. Viesti, E. M. Winchester, and S. J. Yennello, *Phys. Rev. C* **69**, 031604(R) (2004).
- [9] H. Yu, D. Q. Fang, and Y. G. Ma, *Nucl. Sci. Tech.* **31**, 61 (2020).
- [10] Y. G. Ma and W. Q. Shen, *Nucl. Sci. Tech.* **15**, 4 (2004).
- [11] H. L. Liu, Y. G. Ma, and D. Q. Fang, *Phys. Rev. C* **99**, 054614 (2019).
- [12] A. Bonasera, R. Coniglione, and P. Sapienza, *Eur. Phys. J. A* **30**, 47 (2006).
- [13] W. Cassing, V. Metag, U. Mosel, and K. Niita, *Phys. Rep.* **188**, 363 (1990).
- [14] Y. Schutz (TAPS Collaboration), *Nucl. Phys. A* **630**, 126 (1998).
- [15] G. H. Liu, Y. G. Ma, X. Z. Cai, D. Q. Fang, W. Q. Shen, W. D. Tian, and K. Wang, *Phys. Lett. B* **663**, 312 (2008).
- [16] Y. G. Ma, G. H. Liu, X. Z. Cai, D. Q. Fang, W. Guo, W. Q. Shen, W. D. Tian, and H. W. Wang, *Phys. Rev. C* **85**, 024618 (2012).
- [17] X. G. Deng and Y. G. Ma, *Nucl. Sci. Tech.* **28**, 182 (2017).
- [18] X. G. Deng and Y. G. Ma, *Eur. Phys. J. A* **54**, 204 (2018).
- [19] G. C. Yong and B. A. Li, *Phys. Rev. C* **96**, 064614 (2017).
- [20] H. Nifenecker and J. A. Pinston, *Annu. Rev. Part. Nucl. Sci.* **40**, 113 (1990).
- [21] K. B. Beard, W. Benenson, C. Bloch, E. Kashy, J. Stevenson, D. J. Morrissey, J. van der Plicht, B. Sherrill, and J. S. Winfield, *Phys. Rev. C* **32**, 1111(R) (1985).
- [22] A. Adare *et al.* (PHENIX Collaboration), *Phys. Rev. Lett.* **104**, 132301 (2010).
- [23] S. Turbide, C. Gale, and R. J. Fries, *Phys. Rev. Lett.* **96**, 032303 (2006).
- [24] R. Chatterjee, Evan S. Frodermann, Ulrich Heinz, and Dinesh K. Srivastava, *Phys. Rev. Lett.* **96**, 202302 (2006).
- [25] L. Bhattacharya and P. Roy, *Phys. Rev. C* **78**, 064904 (2008).
- [26] R. Rapp, H. van Hees, and M. He, *Nucl. Phys. A* **931**, 696 (2014).

- [27] C. L. Tam, J. Stevenson, W. Benenson, J. Clayton, Y. Chen, E. Kashy, A. R. Lampis, D. J. Morrissey, M. Samuel, T. K. Murakami, and J. S. Winfield, *Phys. Rev. C* **38**, 2526 (1988).
- [28] M. Kwato Njock, M. Maurel, E. Monnard, H. Nifenecker, J. A. Pinston, F. Schussler, D. Barneoud, and Y. Schutz, *Nucl. Phys. A* **482**, 489 (1988).
- [29] J. Stevenson, K. B. Beard, W. Benenson, J. Clayton, E. Kashy, A. Lampis, D. J. Morrissey, M. Samuel, R. J. Smith, C. L. Tam, and J. S. Winfield, *Phys. Rev. Lett.* **57**, 555 (1986).
- [30] E. Grosse, P. Grimm, H. Heckwolf, W. F. J. Müller, H. Noll, A. Oskarsson, and H. Stelzer, *Europhys. Lett.* **2**, 9 (1986).
- [31] R. Bertholet, M. Kwato Njock, M. Maurel, E. Monnard, H. Nifenecker, P. Perrin, J. A. Pinston, F. Schussler, D. Barneoud, C. Guet, and Y. Schutz, *Nucl. Phys. A* **474**, 541 (1987).
- [32] E. Migneco, C. Agodi, R. Alba, G. Bellia, R. Coniglione, A. Del Zoppo, P. Finocchiaro, C. Maiolino, P. Piattelli, G. Russo, P. Sapienza, A. Badali, R. Barbera, A. Palmeri, G. S. Pappalardo, F. Riggi, A. C. Russo, A. Peghaire, and A. Bonasera, *Phys. Lett. B* **298**, 46 (1993).
- [33] B. A. Remington, M. Blann, and G. F. Bertsch, *Phys. Rev. Lett.* **57**, 2909 (1986).
- [34] B. A. Remington and M. Blann, *Phys. Rev. C* **36**, 1387 (1987).
- [35] C. M. Ko and C. Y. Wong, *Phys. Rev. C* **33**, 153 (1986).
- [36] K. Nakayama and G. Bertsch, *Phys. Rev. C* **34**, 2190 (1986).
- [37] T. S. Biro, K. Niita, A. L. De Paoli, W. Bauer, W. Cassing, and U. Mosel, *Nucl. Phys. A* **475**, 579 (1987).
- [38] C. M. Ko, G. Bertsch, and J. Aichelin, *Phys. Rev. C* **31**, 2324(R) (1985).
- [39] K. Niita, A. L. De Paoli, W. Bauer, T. S. Biro, W. Cassing, and U. Mosel, *Nucl. Phys. A* **482**, 525 (1988).
- [40] W. Bauer, G. F. Bertsch, W. Cassing, and U. Mosel, *Phys. Rev. C* **34**, 2127 (1986).
- [41] W. Cassing, T. Biro, U. Mosel, M. Tohyama, and W. Bauer, *Phys. Lett. B* **181**, 217 (1986).
- [42] D. T. Khoa, N. Ohtsuka, S. W. Huang, M. Ismail, A. Faessler, M. El Shabshiry, and J. Aichelin, *Nucl. Phys. A* **529**, 363 (1991).
- [43] F. M. Marqués, G. Martínez, Y. Schutz, J. Díaz, M. Franke, S. Hlaváč, R. Holzmann, P. Lautridou, F. Lefèvre, H. Löhner, A. Marín, T. Matulewicz, W. Mittig, R. W. Ostendorf, J. H. G. van Pol, J. Québert, P. Roussel-Chomaz, A. Schubert, R. H. Siemssen, R. S. Simon, Z. Sujkowski, V. Wagner, H. W. Wilschut, and Gy. Wolf, *Phys. Lett. B* **349**, 30 (1995).
- [44] G. Martínez, F. M. Marqués, Y. Schutz, Gy. Wolf, J. Díaz, M. Franke, S. Hlaváč, R. Holzmann, P. Lautridou, F. Lefèvre, H. Löhner, A. Marín, T. Matulewicz, W. Mittig, R. W. Ostendorf, J. H. G. van Pol, J. Québert, P. Roussel-Chomaz, A. Schubert, R. H. Siemssen, R. S. Simon, Z. Sujkowski, V. Wagner, and H. W. Wilschut, *Phys. Lett. B* **349**, 23 (1995).
- [45] P. Danielewicz, *Acta. Phys. Pol. B* **33**, 45 (2002).
- [46] D. D. S. Coupland, W. G. Lynch, M. B. Tsang, P. Danielewicz, and Y. X. Zhang, *Phys. Rev. C* **84**, 054603 (2011).
- [47] J. Aichelin, *Phys. Rep.* **202**, 233 (1991).
- [48] C. Hartnack, R. K. Puri, J. Aichelin, J. Konopka, S. A. Bass, H. Stöcker, and W. Greiner, *Eur. Phys. J. A* **1**, 151 (1998).
- [49] L. W. Chen, F. S. Zhang, and G. M. Jin, *Phys. Rev. C* **58**, 2283 (1998).
- [50] T. Z. Yan and S. Li, *Nucl. Sci. Tech.* **30**, 43 (2019).
- [51] T. T. Wang, Y. G. Ma, and Z. Q. Zhang, *Phys. Rev. C* **99**, 054626 (2019).
- [52] T. Z. Yan, S. Li, Y. N. Wang, F. Xie, and T. F. Yan, *Nucl. Sci. Tech.* **30**, 15 (2019).
- [53] P. C. Li, Y. J. Wang, Q. F. Li, and H. F. Zhang, *Nucl. Sci. Tech.* **29**, 177 (2018).
- [54] A. Ono, J. Xu, M. Colonna *et al.*, *Phys. Rev. C* **100**, 044617 (2019).
- [55] Z. F. Zhang, D. Q. Fang, and Y. G. Ma, *Nucl. Sci. Tech.* **29**, 78 (2018).
- [56] Z. Q. Feng, *Nucl. Sci. Tech.* **29**, 40 (2018).
- [57] S. Sood, R. Kumar, A. Sharma, and R. K. Puri, *Phys. Rev. C* **99**, 054612 (2019).
- [58] Y. X. Zhang, Y. J. Wang, M. Colonna, P. Danielewicz, A. Ono, M. B. Tsang, H. Wolter, J. Xu, L. W. Chen, D. Cozma, Z. Q. Feng, S. Das Gupta, N. Ikeno, C. M. Ko, B. A. Li, Q. F. Li, Z. X. Li, S. Mallik, Y. Nara, T. Ogawa, A. Ohnishi, D. Oliinychenko, M. Papa, H. Petersen, J. Su, T. Song, J. Weil, N. Wang, F. S. Zhang, and Z. Zhang, *Phys. Rev. C* **97**, 034625 (2018).
- [59] O. Lopez, D. Durand, G. Lehaut, B. Borderie, J. D. Frankland, M. F. Rivet, R. Bougault, A. Chbihi, E. Galichet, D. Guinet, M. La Commara, N. Le Neindre, I. Lombardo, L. Manduci, P. Marini, P. Napolitani, M. Parlog, E. Rosato, G. Spadaccini, E. Vient, and M. Vigilante, *Phys. Rev. C* **90**, 064602 (2014).
- [60] G. Q. Li and R. Machleidt, *Phys. Rev. C* **48**, 1702 (1993).
- [61] G. Q. Li and R. Machleidt, *Phys. Rev. C* **49**, 566 (1994).
- [62] K. Chen, Z. Fraenkel, G. Friedlander, J. R. Grover, J. M. Miller, and Y. Shimamoto, *Phys. Rev.* **166**, 949 (1968).
- [63] J. D. Jackson, *Classical Electrodynamics* (Wiley, New York, 1962), p. 733.
- [64] C. A. Ogilvie, J. C. Adloff, M. Begemann-Blaich, P. Bouissou, J. Hubele, G. Imme, I. Iori, P. Kreutz, G. J. Kunde, S. Leray, V. Lindenstruth, Z. Liu, U. Lynen, R. J. Meijer, U. Milkau, W. F. J. Muller, C. Ngo, J. Pochodzalla, G. Raciti, G. Rudolf, H. Sann, A. Schuttauf, W. Seidel, L. Stuttge, W. Trautmann, and A. Tucholski, *Phys. Rev. Lett.* **67**, 1214 (1991).
- [65] R. K. Puri and S. Kumar, *Phys. Rev. C* **57**, 2744 (1998).
- [66] R. Alba, C. Maiolino, C. Agodi, A. Del Zoppo, R. Coniglione, P. M. Milazzo, P. Sapienza, G. Bellia, M. Bruno, M. Colonna, N. Colonna, M. D'Agostino, M. L. Fiandri, P. Finocchiaro, F. Gramegna, I. Iori, K. Loukachine, G. V. Margagliotti, P. F. Mastinu, E. Migneco, A. Moroni, P. Piattelli, R. Rui, D. Santonocito, F. Tonetto, and G. Vannini, *Nucl. Phys. A* **654**, 761c (1999); **681**, 339 (2001).
- [67] D. G. D'Enterria, G. Martínez (For the TAPS Collaboration), *Czech. J. Phys.* **50**, Suppl. 4, 103 (2000).
- [68] D. G. D'Enterria, G. Martínez, L. Aphecetche, H. Delagrange, F. Fernández, H. Löhner, R. Ortega, R. Ostendorf, Y. Schutz, and H. W. Wilschut, *Phys. Lett. B* **538**, 27 (2002).
- [69] F. Zhang, C. Li, P. W. Wen, J. W. Liu, J. Su, and F. S. Zhang, *Phys. Rev. C* **100**, 024603 (2019).